

1N-14  
131754  
P.42

# Nonconservative Force Model Parameter Estimation Strategy for TOPEX/Poseidon Precision Orbit Determination

S. B. Luthcke and J. A. Marshall

(NASA-TM-104575) NONCONSERVATIVE  
FORCE MODEL PARAMETER ESTIMATION  
STRATEGY FOR TOPEX/POSEIDON  
PRECISION ORBIT DETERMINATION  
(NASA) 42 p

N93-13372

Unclass

G3/14 0131754

November 1992

**NASA**



**NASA Technical Memorandum 104575**

**Nonconservative Force Model  
Parameter Estimation Strategy  
for TOPEX/Poseidon Precision Orbit  
Determination**

**S. B. Luthcke**  
*Hughes STX Corporation*  
*Lanham, Maryland*

**J. A. Marshall**  
*Goddard Space Flight Center*  
*Greenbelt, Maryland*



National Aeronautics and  
Space Administration

**Goddard Space Flight Center**  
Greenbelt, Maryland 20771



# NONCONSERVATIVE FORCE MODEL PARAMETER ESTIMATION STRATEGY FOR TOPEX/POSEIDON PRECISION ORBIT DETERMINATION

S. B. Luthcke<sup>1</sup>  
J. A. Marshall<sup>2</sup>

## Abstract

The TOPEX/Poseidon spacecraft was launched on August 10, 1992 to study the Earth's oceans. To achieve maximum benefit from the altimetric data it is to collect, mission requirements dictate that TOPEX/Poseidon's orbit must be computed at an unprecedented level of accuracy. To reach our pre-launch radial orbit accuracy goals, the mismodeling of the radiative nonconservative forces of solar radiation, Earth albedo and infrared re-radiation, and spacecraft thermal imbalances cannot produce in combination more than a 6 cm rms error over a 10 day period. Similarly, the 10-day drag modeling error cannot exceed 3 cm rms. In order to satisfy these requirements, a "box-wing" representation of the satellite has been developed in which, the satellite is modelled as the combination of flat plates arranged in the shape of a box and a connected solar array. The radiative/thermal nonconservative forces acting on each of the eight surfaces are computed independently, yielding vector accelerations which are summed to compute the total aggregate effect on the satellite center-of-mass. Select parameters associated with the flat plates are adjusted to obtain a better representation of the satellite acceleration history. This study analyzes the estimation of these parameters from simulated TOPEX/Poseidon laser data in the presence of both nonconservative and gravity model errors. A "best choice" of estimated parameters is derived and the ability to meet mission requirements with the "box-wing" model evaluated.

---

<sup>1</sup>Hughes STX, Lanham, Maryland

<sup>2</sup>NASA Goddard Space Flight Center, Space Geodesy Branch, Greenbelt, Maryland

## INTRODUCTION

### Mission/Science Overview

The Ocean TOPography EXperiment/Poseidon Mission (T/P), is a joint venture between the U.S.'s National Aeronautics and Space Administration (NASA) and the French Centre National d'Etudes Spatiales (CNES). T/P was launched on August 10, 1992 aboard the European Space Agency's Ariane launch vehicle. The TOPEX/Poseidon spacecraft is equipped with two radar altimeters (1 US, and 1 French), which measure the ocean surface topography. Radar altimeters measure the height of a satellite above the ocean surface yielding a continuous observation of the sub-satellite sea surface height within a geocentric reference frame. After accounting for both the geoid height and Earth/ocean tides, a measure of the ocean's dynamic topography is obtained. Knowledge of the dynamic topography is very important for monitoring the surface geostrophic currents and the ocean's thermal response which drive global weather patterns and their changes. Understanding the ocean-climate interaction, phenomena such as the El Nino, and monitoring possible mean sea level rise due to global warming are part of the scientific objectives of the T/P Mission.

### Precision Orbit Determination

The T/P spacecraft orbits the Earth at an altitude of 1336 km, inclination of  $66^{\circ}$  and with nearly zero eccentricity. The period of the orbit is 1.87 hours and its groundtrace repeats every 10 days to within +/- 1 km in a "frozen" orbit. Since the orbit of T/P provides the absolute reference frame for the altimeter measurements, any error in determining the satellite's position will affect the direct measure of sea surface height. In order to obtain measurements of dynamic topography to the degree of accuracy that is required for several core oceanographic investigations, 13 cm RMS radial orbit accuracy over contiguous 10 day periods with less than 5 cm RMS geographically correlated error is sought (*Stewart et al., 1986*). Orbit determination of this accuracy presents many challenges for it has never before been achieved for a satellite at T/P's altitude.

Until recently, gravity field mismodeling was the major source of error in precise orbit definition. However, with improvements in these models through the support of the TOPEX Project, geopotential error has been considerably reduced (*Marsh et al., 1990; Lerch et al., 1992*). Accurate modeling of the nonconservative forces on T/P has become a significant concern (*Ries et al., 1992*). To achieve the T/P radial orbit modeling goals, it is no longer prudent to ignore the rotating, attitude controlled, geometrically complex shape of T/P. Given the former dominating nature of geopotential errors and the lower altitudes of former altimeter missions, it has been common to represent these satellites as symmetrically perfect and rotationally invariant spheres (i.e. so-called "cannonball" models; cf. *Haines et al.,*

1990) in the evaluation of surface forces. When using this computationally simple model, empirical acceleration-scaling parameters were adjusted to achieve good quality orbit accuracies. These empirical terms were nominally of three types. First, in the cannonball representation, the area-to-mass is assumed invariant. Therefore,  $C_D$  and  $C_R$ , which act as scaling factors on the drag and solar radiation accelerations respectively, are adjusted to assure the proper estimation of the mean semi-major axis in the orbital state solution over the entire orbit, or for shorter prescribed intervals. Furthermore, 1 cycle-per-revolution (1CPR) empirical accelerations have recently been added to the arsenal of empirical parameters used to accommodate the mismodeling of these non-conservative forces. The terms are especially effective in reducing orbit error in circumstances where the drag effect is large and piecewise discontinuous  $C_D$  terms cannot adequately address the systematic errors in the atmospheric density modeling within each orbital revolution. These 1 CPR acceleration terms are normally adjusted as aggregate values within the orbit solution.

Atmospheric drag is of considerably less concern at TOPEX/Poseidon's altitude. It is suspected that since a "cannonball" modeling approach neglects T/P's complex projected area and surface properties, the long wavelength ocean topography features can be aliased into the recovered empirical terms. It is therefore desirable to minimize general radiation pressure scaling parameters when modeling the radiation forces acting on T/P. Therefore, additional analysis of the T/P nonconservative forces has been undertaken and resultant source-specific parameters have been assessed.

*Antreasian (1992)* performed a detailed 310-node finite element analysis of the spacecraft to produce acceleration histories for each of the radiative forces (solar radiation, Earth albedo/IR, and thermal imbalance). These complex acceleration histories, known as "micro-models", were adopted for analysis. *Marshall et al. (1991)* developed a less computationally intensive model suitable for use in precision orbit determination. This "box-wing" or "macro-model" represents the satellite as the combination of flat plates arranged in the shape of a box and a connected solar array which follow the T/P nominal attitude control laws. The nonconservative forces acting on each of the eight surfaces are computed independently, yielding vector accelerations which are summed to compute the total aggregate effect on the satellite center-of-mass. Composite parameters associated with each plate needed for this model have been obtained through least square fits to the micro-models. The tracking data acquired on T/P will be used to further improve these parameters. The optimal design of solutions for these plate-specific parameters is the focus of this study.

## "Box-Wing" Macro-Model of the TOPEX/Poseidon Spacecraft

Figure 1 shows the "box-wing" representation of the TOPEX/Poseidon spacecraft. There are eight flat plates used in the approximation consisting of 6 for the box and 1 each for the front and back of the solar array. In the following discussions the individual plates comprising the macro-model will be identified by their body fixed direction. For example, X- represents the box plate whose normal is directed outward from the spacecraft along the X- axis and SA+ represents the solar array cell side (see *Marshall et al., (1991)* for a complete description of the "macro-model"). The following list describes the parameters associated with each plate in the macro-model:

- Area
- Specular Reflectivity
- Diffuse Reflectivity
- Emissivity
- Cold Equilibrium Temperature
- Temperature Differential between Hot & Cold Equilibrium Temp.
- Exponential Decay Time for Panel Cooling
- Exponential Decay Time for Panel Heating
- Temperature/Satellite Rotation Scale Factor

The pertinent acceleration equations can be found in Appendix A. Values for the above were computed by fitting each force (solar, thermal imbalance, Earth albedo and IR) to the micro-model accelerations yielding the a priori values listed in *Marshall et al., (1992)*. Thus, when a parameter is held fixed within an orbit solution, it is this a priori value which is used.

The sun-Earth-T/P orbit geometry can be represented using two parameters.  $\beta'$  refers to the angle between the sun vector and the orbit plane as shown in Figure 2. The T/P attitude control "laws" change from sinusoidal to fixed yaw over certain regimes of  $\beta'$ . The orbit angle  $\Omega$  is measured from the inertial coordinate system  $Y_0$ -axis. A detailed description of the TOPEX/Poseidon Yaw-steering attitude control as a function of  $\beta'$  and  $\Omega$  is also given in *Marshall et al., 1991*.

### Initial Simulations

After the "macro" model was implemented into the GEODYN precision orbit determination software package at NASA/GSFC (*Putney et al., 1991*), a study was initiated to validate this model. A brief summary of the methodology and results of this investigation is presented here for it forms the basis of subsequent analyses. A more detailed discussion can be found in *Marshall et al., 1992*.

The micro-model acceleration histories, being the product of a 310-node finite element analysis, were adopted as a "truth" model. GEODYN was modified to ingest the micro-model acceleration histories and apply the appropriate value for each of the forces at every integration step (using a bilinear interpolation over  $\beta'$  and  $\Omega$ ). For the initial study satellite cartesian position and velocity data (so called "Precise Cartesian Element" - PCE) was simulated using the micro-models. The simulated data covered a 10 day arc that spanned the  $\beta'$  region of  $10^\circ$  to  $39^\circ$ . This arc was chosen for it spans the complex fixed yaw to sinusoidal yaw transition regime. A 30 second integration step size was used for all simulations and the data generation interval was 180 seconds. This data was then used as input into a second GEODYN run which used the "box-wing" concept to model the non-conservative forces acting on T/P. The resulting residuals represent the macro-model's error in reproducing the micro-model. This simulation was used to gauge the anticipated modeling errors with their temporal characteristics that will likely be observed when processing actual T/P data.

Each of the individual radiative forces (solar radiation, thermal imbalance, Earth albedo and IR) were considered separately. Only the orbit state, and a single drag and solar radiation pressure coefficient were adjusted over the 10 day arc interval. The radial rms orbit error was computed from the residuals of the macro-model orbit fit to the micro-model PCE data. Table 1 gives the modelability and error analysis summary. It shows that with no adjustment of the macro-model surface specific parameters and a minimal adjusted parameter set, the individual macro-model errors each meet the 6 cm radial rms mission requirement. However, when the combined contribution of all the radiative forces was considered the radial rms orbit error rose to 7.0 cm.

Although initially useful in gaining insight into the characteristics of the anticipated T/P orbit errors, this study has four major deficiencies. First, simulated PCE data provides continuous three dimensional satellite positioning which is unavailable from the mission baseline laser tracking. Therefore, the simulation did not address the sparse temporal distribution and geometry provided by laser tracking. The tracking data provided by the laser network must be capable of meeting Mission requirements and "tuning" the macro-models. Second, only the  $\beta'$  region of  $10^\circ$  to  $39^\circ$  was investigated. Acceleration characteristics show significant variation over the  $0^\circ$  to  $88^\circ$   $\beta'$  regime with changes in the spacecraft attitude control algorithms and Sun-orbit plane geometry. The negative  $\beta'$  regions are assumed to be symmetric to their positive counterparts and, therefore, no micro-model acceleration histories exist for this region. Third, none of the T/P "box-wing" specific parameters were used in the adjustments. Thus improved model parameter recovery needs to be addressed. Finally, the radiative/thermal surface force model was not examined in the presence of other orbit error sources such as drag and/or the geopotential.

## RADIATIVE FORCE MODEL ERRORS

### Laser Data Simulations

In order to address the above shortcomings, a second investigation was initiated. This study used simulated data that represents a nominal T/P laser tracking scenario. Orbit errors for four separate 10 day arcs that represent  $\beta'$  regions between  $0^\circ$  and  $88^\circ$  were investigated. Macro-model radial orbit errors were quantified using two different parameter adjustment strategies to fit the simulated data generated using the micro-models. The first approach used no a priori constraints on the adjusted subset of macro-model parameters when fitting the simulated laser data over all  $\beta'$  regions. The second approach allowed all of the "box-wing" parameters (except temperature parameters) to adjust with a set of realistic a priori constraints. Finally, orbit errors induced from the mismodeling of the radiative, drag, and gravity forces acting in combination were considered. Through these simulations, our understanding of the "box-wing" parameter recovery and correlations has been greatly improved.

Data for this investigation was simulated for four 10 day arcs using the baseline station configuration and tracking scenario as described in the Crustal Dynamics Satellite Laser Ranging Network Topex/Poseidon Laser Network Support Plan (*Murdoch and Decker, 1989*) and shown in Table 2. Stations in baseline network will be staffed with two 8 hour/5 day per week shifts. The first shift will track T/P as its top priority while the second shift will assign it a somewhat lower priority. In order to account for some of the data losses due to weather and down time, we assume that the first shift will obtain 40% of the possible passes while the second shift obtains 20%. The two days at 20% tracking attempt to address the expected decrease in tracking during the weekend. It is important to note that not all of the complexity of an actual Topex tracking scenario is represented in this simulation schedule. For example, we assumed that all stations start and stop their tracking at the same time and no station time zones were used. Priority shifts do not overlap and start consecutively for all stations. This scenario generates an average of 190 passes per 10 day arc which is a reasonable quantity of data as confirmed now that actual laser tracking of T/P has commenced.

### Parameter Recoverability and Separability

In order to investigate "box-wing" parameter performance and characteristics, many simulations with various combinations of adjusted "box-wing" parameters were made. It should be noted that in all of the simulations in this analysis the initial orbit state is always adjusted together with the specified parameters being investigated. All of the temperature related parameters used in the thermal imbalance acceleration model were held fixed during testing. Initial simulations

demonstrated that these parameters are poorly determined if adjusted. The partials of thermal imbalance acceleration are a function of the third power of temperature and are highly non-linear. Thus the temperature parameters are highly dependent on a priori information. Also, the thermal imbalance is a function of the temperature gradient between surfaces rather than a single plate's temperature. Laser tracking data tends to have significant gaps in coverage and the weak temperature change signal associated with any one plate is not resolved.

As described previously, the simulations fit a macro-model parameterized orbit to micro-model simulated laser tracking data for four 10 day arcs that span the following  $\beta'$  regions:  $0^\circ$  to  $29^\circ$ ,  $10^\circ$  to  $39^\circ$ ,  $39^\circ$  to  $68^\circ$ ,  $67^\circ$  to  $88^\circ$ . The first approach used (a) the solution variances, (b) the correlation between adjusted parameters, and (c) a parameter's relative impact on the data fit; as criteria to define the minimum set of freely adjusting macro-model parameters that best reduced the radiative force mismodeling residuals over the complete range of  $\beta'$  values. Again, these simulations are done in computations supported exclusively by simulated laser tracking. This parameter set is termed the "free adjustment set"; to reiterate, this parameter set is used to best fit data over **all**  $\beta'$  regions.

This new set of simulations clearly demonstrated the capabilities and limits of macro-model parameter recoverability and separability. Certain terms were highly correlated in all  $\beta'$  regions. For example, emissivities on opposite faces are always highly correlated because their dynamic partial derivatives differ by only a multiplicative factor, namely the negative of the temperature gradient. Also, there is no specific geometry or visibility dependence to help separate these parameters. The SA+ diffuse reflectivity, SA+ specular reflectivity, and the SA+ area are also correlated since the solar array normal vector is always nearly parallel to the solar incidence vector. Consequently, the dynamic partials of these parameters only differ by a multiplicative factor.

A main factor in the parameter estimability is the varying spacecraft attitude (*Zimbelman, 1989*). Therefore, parameter recovery and its effect on the reduction of the orbit error is a function of  $\beta'$  and it is extremely difficult to derive a single set of parameters which behave well in all regions. The SA+ reflectivities (diffuse and specular) and SA+ emissivity can be separated in the low  $\beta'$  region due to the occultation/visibility dependence of the SA+ specular reflectivity. However, at  $\beta' > 56^\circ$  the visibility dependence is eliminated as the spacecraft is no longer occulted by the Earth and it becomes much harder to separate the two terms since both directly scale the forces acting in a direction normal to the solar array. Similarly, all area parameters have separability and visibility problems in some  $\beta'$  region. For example, in high  $\beta'$  regions the X- area is correlated with the X-specular, X-diffuse, SA+ specular, SA+ diffuse, SA+ emissivity, and SA+ area, because they are all pointing in the same sun pointing direction. The X+

parameters are not very observable since there is no solar visibility above  $\beta'$  of  $15^\circ$  and the exposure to earth radiation pressure is minimal and decreases as  $\beta'$  increases. The Z- diffuse reflectivity is correlated with the Z- specular reflectivity in the low  $\beta'$  region where they both contribute to accelerations that have strong signals in the solar pointing direction. Because of the near uniform earth radiation pressure at low  $\beta'$  (full illumination of visible earth - no occultation offset) the Z+ diffuse and Z+ specular reflectivity parameters are hard to separate in this low  $\beta'$  region. The Y- plate has some solar visibility in all  $\beta'$  regions, and its diffuse reflectivity parameter can be recovered. Above  $\beta'$  of  $15^\circ$  the Y+ plate is solar visible, and in this region the specular reflectivity for this plate is well determined. The Y plates have a very strong solar visibility variation over all  $\beta'$  regions. This helps to separate specular and diffuse reflectivities, and emissivities in all  $\beta'$  regions. However, as we shall see later, emissivity parameters for the Y plates are highly correlated with  $C_D$  (drag coefficients) in the high  $\beta'$  regions where the Y plates are predominantly facing in the along track direction. This summary gives a flavor of the lessons learned in deriving the following free-adjustment parameter set:

- |                                 |                              |
|---------------------------------|------------------------------|
| <b>1) SPECULAR REFLECTIVITY</b> | <b>▸ X-, Y+, Z+, Z-, SA-</b> |
| <b>2) DIFFUSE REFLECTIVITY</b>  | <b>▸ Y-, SA+</b>             |
| <b>3) EMISSIVITY</b>            | <b>▸ X-, Y+, SA+</b>         |

This is not to say that the free-adjustment parameter set is perfect. When these parameters are allowed to adjust freely some of the recovered values are not physically realistic (ie. specular reflectivity values or emissivity values greater than one). This indicates that the free-adjustment subset is soaking up additional errors not directly related to the adjusted parameters. Additionally, minor separability problems still exist but were tolerated because of the parameter's ability to improve the fit to the simulated data. For example, the SA+ diffuse reflectivity and SA+ emissivity above  $\beta'$  of  $56^\circ$  are both nearly pointing in the Sun incidence direction without any visibility separation. Therefore, with a small amount of tracking data these two parameters may not be separated. These separability problems can be rectified by either producing a parameter subset for each  $\beta'$  region or by eliminating some of the parameters at some cost to the orbit performance.

The second approach was to use a "realistic" set of constraints and allow all of the non-temperature parameters to adjust. The constrained parameter set is:

- |                                 |                                    |
|---------------------------------|------------------------------------|
| <b>1) SPECULAR REFLECTIVITY</b> | <b>▸ X+,X-,Y+,Y-,Z+,Z-,SA+,SA-</b> |
| <b>2) DIFFUSE REFLECTIVITY</b>  | <b>▸ X+,X-,Y+,Y-,Z+,Z-,SA+,SA-</b> |
| <b>3) EMISSIVITY</b>            | <b>▸ X+,X-,Y+,Y-,Z+,Z-,SA+,SA-</b> |
| <b>4) AREA</b>                  | <b>▸ X+,X-,Y+,Y-,Z+,Z-,SA+,SA-</b> |

The constraints represent an attempt to quantify the parameter maximum error bounds that can be expected on orbit. The area constraints selected were 0.5 meters for the box and 0.1 meters for the solar array front and back. The standard deviation (0.3) of the beginning of life (BOL) and end of life (EOL) material properties for the major materials on the box served to define the error bounds for the specular and diffuse reflectivity of the box plates. The behavior of the solar array materials is relatively well known and a pessimistic estimate of the difference (0.1) between BOL and EOL values was used to constrain the solar array front and back diffuse and specular reflectivities. Material tests indicate that emissivity values do not vary significantly over the mission lifetime but the error bounds were set at 0.1 to help accommodate errors in the computation of the temperature gradient. Information on material properties was obtained from *O'Donnell and Whitt (1992)* and *O'Donnell et al. (1991)*. Simulations were made fitting the aforementioned constrained set of macro-model parameters to the micro-model simulated laser data as before. The benefit of this approach is that it breaks correlations and gives physically realistic parameter solutions. The danger here is that the data's ability to specify the parameter value is restricted and, instead, the a priori information makes a significant contribution to least squares orbit fit.

## Results

The results of these simulations are tabulated in Tables 3 and 4. The free-adjusting parameter set produces better fits to the simulated data as compared to the constrained set of parameters. Evidently, the parameters constraints are restrictive enough to prohibit the adjustment required to absorb the entire error signal. Most importantly, however, both approaches produce radial orbit error well under the 6 cm mission requirement. *Marshall et al. (1992)* demonstrated that without any "box-wing" parameter adjustment, the radial acceleration residuals were highest in the low  $\beta'$  regime and the cross track modeling was poor in the high  $\beta'$  region. The constrained parameter set follows this radial trend because the solar array parameters are over-constrained. The opposite is true for the free-adjustment parameter set which produces its best radial fit in the low  $\beta'$  regions and a good fit to the cross track signal for the high  $\beta'$  region.

The  $0^\circ$  to  $29^\circ$   $\beta'$  regions radial fit is slightly worse than the  $10^\circ$  to  $39^\circ$   $\beta'$  region due to the fact that radial and along track acceleration residuals are highest in the  $0^\circ$  to  $29^\circ$  region. In low  $\beta'$  the sun incidence vector and, therefore, the solar array are aligned predominantly in the radial direction. The strong solar array parameters and the Z plate terms do an excellent job of accommodating the radial error signal in this region.

As the orbit moves to higher  $\beta'$  regions, the solar array tends to align with the cross track direction and, as a result, the cross track fit remains stable even though the

actual acceleration increases dramatically. The exception to this trend falls in the  $\beta'$  region of  $39^\circ$  to  $68^\circ$ . This can be attributed to the large acceleration residual spikes occurring at a  $\beta'$  of  $56^\circ$  where T/P moves into a full sunlight orbit (Marshall *et al.*, 1992). These spikes are an artifact due to differences in the occultation boundary definition between the macro and micro-models as well as the instantaneous, and in some cases discontinuous, transitions between plate temperature algorithms in the macro-model. Reduction of these residual spikes through parameter adjustment is difficult.

Finally, for completeness, an additional simulation using 100% visibility for the simulated laser tracking was made. The results of this simulation is shown in Table 3 and demonstrate that, as expected, improved data coverage will significantly improve the modelability of all of the non-conservative radiative forces. The DORIS and GPS tracking systems aboard T/P offer tracking coverage which is similar in character to this simulated data set (Dorrer, 1990, Melbourne and Davis, 1987).

In the set of simulation described to this point, the force model error which was examined is attributable to the differences between the macro and micro-model acceleration histories. Since the results are based on the assumption that the micro-models represent truth, it is important to investigate the performance of the above parameterizations in the presence of other plausible descriptions of radiative errors. To this end, macro-model parameter values were perturbed in a Monte-Carlo manner by amounts equivalent to the error bounds previously discussed to produce two additional "clone" error models. A third error model was created through similar perturbations so as to create the maximum net accelerations, and thus maximum errors, in a particular direction. Only two of the  $\beta'$  regimes were evaluated when fitting the macro-model parameterizations to simulated nominal laser data created using these error models. As shown in Table 4, the resulting orbit errors are much smaller than those obtained by fitting the micro-model simulated data. The explanation lies in the fact that these "clone" error models are based on homogeneous plate characteristics. In reality, as in the micro-models, each plate is made up of assorted materials which all have different surface properties. It is, therefore, expected that the macro-model would better mimic the characteristics of the "clone" models. Note that, as expected, the "clone" error model with the maximum accelerations shows the poorest fit performance. These error models use very pessimistic error bounds.

### **RADIATIVE FORCE MODEL and ATMOSPHERIC DENSITY MODEL ERRORS**

To continue the examination of the "box-wing" model's interaction with other error sources, a drag error was introduced into the error model. The "box-wing" model includes the capability to accurately compute the spacecraft projected area in

the velocity direction for any attitude configuration. Therefore, for this investigation, the computation of atmospheric density itself was considered the major error source. Laser tracking data was again simulated using the micro-model radiative acceleration histories and the DTM atmospheric density model, which uses 3-hourly geomagnetic activity indices (*Barlier et al., 1978*). This simulated data was then fit using the earlier Jacchia 1971 (J71) model which is driven by daily geomagnetic activity values (*Jacchia 1971*). The differences in the density models and, specifically the differences in the geomagnetic activity resolution, produce significant errors that can be representative of an actual density computation error (*Ries et al., 1992*).

In order to accommodate the atmospheric density error a drag coefficient ( $C_D$ )-per-day was adjusted. Additionally, the "free-adjustment" subset of macro-model parameters was further reduced to include only the strongest parameters and to eliminate previously discussed separability problems and those associated with the  $C_D$  terms. A solar radiation pressure coefficient ( $C_R$ ) was not adjusted since it is highly correlated with the SA+ specular reflectivity. The reduced set of macro-model parameters allowed to freely adjust in this analysis were as follows:

- |                          |                |
|--------------------------|----------------|
| 1) SPECULAR REFLECTIVITY | ▸ Y+, SA+, SA- |
| 2) EMISSIVITY            | ▸ X-, SA+      |

Additional simulations using more traditional parameterizations were also conducted for completeness. Specifically, the macro-model terms were held fixed during the adjustment of  $C_D$ -per-day,  $C_R$ -per-arc, and 1CPR alongtrack acceleration parameters. This same adjustment set was used with a cannonball representation of the spacecraft. Model performance was evaluated only in the low  $\beta'$  regime for these cases.

## Results

The results of this analysis are documented in Table 5. The first point to stress is that, even with the additional error source, the macro-model still meets, and even exceeds, mission requirements. Notice that the radial orbit error trend in  $\beta'$  has reversed from the radiative error only simulation. The poor performance in the low  $\beta'$  region is attributed to the elimination of the Z+ and Z- specular reflectivity and the SA+ diffuse reflectivity adjustments. The SA+ specular, rather than diffuse, reflectivity was chosen to avoid separability problems with the SA+ emissivity term at high  $\beta'$ . Also, the Y+ emissivity is a very strong parameter for absorbing thermal imbalance errors. However, this term is highly correlated with the  $C_D$  parameters in the high  $\beta'$  regime, where the Y+ plate normal is aligned predominantly in the along track direction. The Y+ specular reflectivity exhibits similar correlation behavior. However, because of its powerful effect on the fits, this term was partially constrained rather than eliminated from the adjustment subset. As

before, the along track error is largest in the low  $\beta'$  region where the radiative macro-micro along track acceleration residuals have traditionally been the largest. Without the adjustment of the Y- diffuse reflectivity and the Y+ emissivity parameters, the cross track error becomes significantly worse in the low  $\beta'$  regions compared to the previous analysis. However, this trend reverses with increasing  $\beta'$  as the Y plate normals rotate into the along track direction and the solar array, and its strong parameters, assume a cross track orientation.

When a 1CPR alongtrack acceleration term was added to the adjusted parameter set, all three components of the orbit error were reduced, as expected. This empirical parameter is designed specifically to absorb any signal at the orbital frequency. Finally, the box-wing parameters were removed from the adjusted parameter set and a  $C_R$ -per-arc term was added. This group of terms was applied to both a simple cannonball and box-wing satellite representation. Both runs showed an approximate 50% improvement in the radial orbit error over the box-wing representation with the macro-model specific parameter adjustment. This would suggest that it is better to hold the box-wing model fixed and adjust for these empirical terms rather than recovering box-wing parameters.

However, the recovered  $C_D$  values exhibited large variations when using the cannonball and 1CPR parameterization, indicating that they were absorbing much of the radiative force modeling error as well as the drag error. Using the reduced free-adjustment macro-model parameter set, the  $C_D$  values remained roughly constant over each day's and arc's solution. As intended, the drag coefficients now act as overall scale factors of the total drag acceleration, rather than "sponges" absorbing solar, thermal and Earth albedo/IR mismodeling and the error in the projected area and density models. The empirical terms, especially, the alongtrack 1CPR, will absorb any signal with the appropriate characteristics; given the systematic distribution of the tracking sites geographically, long wavelength orbit aliasing can result from the use of the 1CPR terms due to favoring certain geographic regions at the expense of those providing less tracking in the recovery of these terms.

The macro-model parameterization attempts to model the actual physical radiative force error sources and is far more source-specific. This is especially important during the first six months of the TOPEX/Poseidon mission when the gravity field will be "tuned" through the inclusion of T/P tracking data into the solution. Furthermore, as we shall see in the following simulations, when a set of macro-model parameters is chosen for a specific  $\beta'$  region the performance is better than the 1CPR parameterization.

## RADIATIVE FORCE MODEL, ATMOSPHERIC DENSITY MODEL, and GRAVITY MODEL ERRORS

In this section the performance of the macro-model and the previously derived free-adjustment macro-model parameterization is evaluated in the presence of radiative force, atmospheric density, and gravity model errors. The spectral characteristics of the orbit error are analyzed to investigate the correlation of the non-conservative force models on the gravity signal. Both the macro-model and the gravity model will be tuned to reflect actual TOPEX/Poseidon spacecraft performance during the first six months of the mission. Therefore, it is crucial that aliasing between models be kept at a minimum. For the following simulations gravity error was produced by simulating a nominal T/P laser tracking scenario using the GEM-T2 gravity field (*Marsh et al., 1989*). These data were orbitally reduced using the GEMT2C1 clone. The GEMT2C1 clone represents a gravity field that is one standard deviation away from GEM-T2 in harmonic space (*Nerem et al., 1992*). Drag and radiative force errors, as described previously, were also added.

### Results

The results of this analysis are documented in Table 6 and Figures 3 through 14. In order to gauge the amplitude and characteristics of the gravity error signal, the first simulation only applied the gravity error and adjusted only the orbit initial state. Figure 3 shows the spectral characteristics of the 10 day arc radial orbit error time series for gravity error only. Note that it is dominated by a 1CPR error signal. The second and third simulations added atmospheric density error (DTM-J71) and radiative force modelling error (macro-micro) as described previously.

The initial state,  $C_D$ -per-day, and the reduced free-adjustment set of macro-model parameters were allowed to adjust for the second simulation. The radial orbit error documented in Table 6 for this case demonstrates the macro-model parameterization will meet the 13.7 cm radial orbit error mission requirements in the presence of radiative force, drag, and gravity errors (*Stewart et al., 1986*). In fact the use of the now outdated GEM-T2 gives an upper bound for the error magnitude and significant improvement is expected with the use of now available models and those available after T/P data tuning. Figure 4 presents the spectral characteristics of the radial orbit error time series for this case and Figure 5 displays the difference between Figures 3 and 4. Figure 5 demonstrates that the macro-model parameterization predominantly affects the once-per-rev radial orbit error signal, reducing its magnitude by 14 cm. The rest of the gravity signal structure is preserved.

In the third simulation, the initial state,  $C_D$ -per-day,  $C_R$ -per-arc, and a 1CPR along track general acceleration in conjunction with a cannonball satellite representation rather than a "box-wing" model are used. The spectral characteristics of the radial orbit error for this parameterization is shown in Figures 6 and 7. Again, it is the 1CPR signal that has been predominantly effected, but in this case the parameterization has absorbed nearly 90% of the original gravity error signal. Table 6 indicates that this parameterization yields a smaller radial orbit error than the macro-model case above, but has a much larger total orbit error due to the large along track error. However, the fit to the laser tracking is better than the fit using the macro-model parameterization even though the orbit is much worse.

The reason for the strange situation above is the 1CPR along track acceleration,  $C_D$ -per-day, and  $C_R$ -per-arc parameterization can result in poor, relatively unconstrained orbit adjustments during intervals where there is little tracking to properly determine the appropriate  $C_D$ . Figures 8 through 11 show no anomalous signatures in the radial and cross track orbit error time series. Figure 13 shows the large along track orbit error at the beginning of the 10 day arc. From figure 14 it is obvious to see that this large along track orbit error is due to the sparse tracking data on the first day of the 10 day arc. In this type of parameterization the  $C_D$ 's are "soaking up" the  $\beta'$  modulation of the radiative force model errors, particularly solar radiation pressure. Without sufficient daily data to resolve a particular  $C_D$  the orbit determination is quite poor. However, the macro-model parameters, which are determined on an arc basis, inherently have the  $\beta'$  modulation of the radiative force model accelerations. Since the macro-model parameters are determined on an arc basis there is sufficient data to properly determine these parameters. This simulation stresses the fact that it is much better to model the actual physics of the problem rather than using empirical "soak up" parameters.

Two simulations with sufficient data in the first day of the 10 day arc were made. The results of these simulations are documented in Table 6. The additional data on the first day provides for the proper solution of the first  $C_D$  and therefore a much better along track fit when using the 1CPR along track,  $C_D$ -per-day, and  $C_R$ -per-arc parameterization. The results for the macro-model parameterization do not significantly change. Radial orbit error spectral characteristics are virtually the same as in the previous simulations.

Based upon the last two simulations it might be tempting to think that with a sufficient daily distribution of the tracking data the 1CPR parameterization performs better than the macro-model parameterization. This comparison requires qualification since the macro-model parameterization was chosen for performance in all  $\beta'$  regions and is not specific for the low  $\beta'$  region being studied. A simulation was made and an optimal set of freely adjusting macro-

model parameters was derived for  $\beta' = 0^\circ$  to  $29^\circ$ . The results are tabulated in Table 6 and show the macro-model parameterization gives the smallest orbit error. The optimal set of freely-adjusting macro-model parameters for this low  $\beta'$  region are:

- |                          |               |
|--------------------------|---------------|
| 1) SPECULAR REFLECTIVITY | ▸ Y-, Z-, SA- |
| 2) DIFFUSE REFLECTIVITY  | ▸ Y-, SA+     |
| 3) EMISSIVITY            | ▸ Y+, SA+     |

For completeness the results of several simulations stepping through the addition of various parameterizations, are given in Table 7. Also, results from a simulation using the constrained set of macro-model parameters is shown in Table 7. Again the constrained set does not perform as well as the free-adjusting set. A proper tuning of constraints perhaps would yield better results.

### Conclusion

An extensive pre-launch parameter performance evaluation of the TOPEX/Poseidon spacecraft "box-wing" non-conservative force modeling has been made. Model performance and parameter performance have been evaluated in terms of orbit error using both ideal spacecraft position data (globally distributed) and a realistic decimated laser tracking scenario. Radiative force, drag, and gravity model error sources have all been considered. An optimal free-adjusting parameter set valid for all  $\beta'$  regions has been derived. In all simulations, macro-model performance has met and often exceeded precision orbit determination error requirements.

Cannonball spacecraft representations adjusting empirical 1CPR terms were also analyzed. These models yield small orbit errors but have been shown to suffer from modeling problems when the daily distribution of tracking data is poor. It has been shown that this type of parameterization is not advisable since one may obtain a good fit to the laser tracking data but have serious orbit error problems. Additionally, it has been shown for macro-model parameterization derived for a specific  $\beta'$  the radial orbit error is smaller than the cannonball alternative. It was extremely difficult to find one parameter set that behaved satisfactorily in all regimes. Thus, the macro-model not only is modeling the actual physical forces on the spacecraft but has been shown to be the superior performer. Finally, the addition of DORIS tracking data and its global coverage will have significant and positive impact on orbit determination and parameter recovery.

A pre-launch macro-model parameterization has been derived and proposed for initial mission precision orbit determination. However, this pre-launch performance

evaluation is based on simulations and real time performance maybe quite different. In the latter case this work will serve as a basis of comparison and information in order to make on-orbit decisions about optimal macro-model parameterization and tuning.

## REFERENCES

- Antreasian, P. G., "Precision Radiation Force Modeling for the TOPEX/POSEIDON Mission," PhD. Dissertation, University of Colorado, April, 1992.
- Barlier, F., C. Berger, J. Falin, G. Kockarts, and G. Thuillier, "Atmospheric Model Based on Satellite Drag Data," *Ann. Geophys.*, 34, 9-24, 1978.
- Dorrer, M., Le System DORIS, Cours International de Technologie Spatiale, CNES Report, Toulouse, France, 1990.
- Haines, B.J., G. H. Born, G. W. Rosborough, J. G. Marsh, and R.G. Williamson, "Precise Orbit Computation for the GEOSAT Exact Repeat Mission", *J. Geophys. Res.*, vol. 95(c3), 2871-2885, 1990.
- Jacchia, L. "Revised Static Models of the Thermosphere and Exosphere with Empirical Temperature Profiles," *Spec. Rep. 313*, 87 pp., Smithsonian Astrophys. Obs., Cambridge, Mass., 1970.
- Knocke, P. C., Ries, J. C., and B. D. Tapley, "Earth Radiation Pressure Effects on Satellites," in *Proceedings of the AIAA/AAS Astrodynamics Conference*, Minneapolis, MN, August 15-17, 1988, pp.577-586.
- Lerch, F.J., R.S. Nerem, B.H. Putney, T.L. Felsentreger, B.V. Sanchez, S.M. Klosko, G.B. Patel, R.G. Williamson, D.S. Chinn, J.C. Chan, K.E. Rachlin, N.L. Chandler, J.J. McCarthy, J.A. Marshall, S.B. Luthcke, D.W. Pavlis, J.W. Robbins, S. Kapoor, and E.C. Pavlis, "Geopotential Models of the Earth From Satellite Tracking, Altimeter and Surface Gravity Observations: GEM-T3 and GEM-T3S," NASA Technical Memorandum 104555, 1992.
- Marsh, J.G., F.J. Lerch, B.H. Putney, T.L. Felsentreger, B.V. Sanchez, S.M. Klosko, G.B. Patel, J.W. Robbins, R.G. Williamson, T.E. Engelis, W.F. Eddy, N.L. Chandler, D.S. Chinn, S. Kapoor, K.E. Rachlin, L.E. Braatz, and E.C. Pavlis, "The GEM-T2 Gravitational Model," *J. Geophys. Res.*, vol. 95, pp.22043-22071, 1990.
- Marshall, J.A, S.B. Luthcke, P. G. Antreasian, and G.W. Rosborough, "Modeling Radiation Forces Acting on Satellites for Precision Orbit Determination," AAS-91-357, AAS/AIAA Astrodynamics Conference, August 1991.
- Marshall, J.A, S.B. Luthcke, P. G. Antreasian, and G.W. Rosborough, "Modeling Radiation Forces Acting on TOPEX/Poseidon for Precision Orbit Determination," NASA Technical Memorandum 104564, June 1992 (submitted to *Journal of Spacecraft and Rockets*).

Melbourne, W. and E.S. Davis, "GPS-Based Precision Orbit Determination: A TOPEX Flight Experiment," AAS/AIAA Astrodynamics Specialist Conference, Paper AAS 87-430, Kalispell, Montana, 1987.

Milani, A., A.M. Nobili, and P. Farinella, *Non-Gravitational Perturbations and Satellite Geodesy*, Adam Hilger, 1987.

Murdoch, A. and W. Decker, "Crustal Dynamics Satellite Laser Ranging Network Support Plan", Goddard Space Flight Center Report CDSLR-03-0002, December 1989.

Nerem, R.S., F.J. Lerch, S.M. Klosko, G.B. Patel, R.G. Williamson, C.J. Koblinsky, "The Absolute Ocean Topography Relative To The Geoid From Satellite Altimetry Based On The GEM-T3 Gravity Model", submitted to JGR, Sept. 1992.

O'Donnel, T., and R. Whitt, "Beginning of Life (BOL) Thermal-Optical Properties of TOPEX Surfaces: Precision Orbit Determination (POD)", JPL Interoffice Memorandum 35592RW.084, July 21, 1992.

O'Donnel, T., R. Whitt, and T. Jones, "TOPEX/Poseidon Precision Orbit Determination (POD): Spacecraft Thermal Properties", JPL Task Implementation Plan, October 31, 1991.

Perrygo, C., "TOPEX Satellite Yaw Maneuvers," Fairchild IOC REF: 968:SE:87-074, 11 November 1987.

Putney, B. H. et al., "GEODYN II System Description," STX Contractor Report, Lanham, MD, 1991.

Ries, J., C. Shum, and B. Tapley, "Surface Force Modeling for Precision Orbit Determination," IUGG XX General Assembly, Symposium U15, August, 1992 (in press).

Stewart, R., Fu, L. L., and M. Lefebvre, "Science Opportunities from the TOPEX/Poseidon Mission," JPL Pub. 86-18, July 1986.

Zimbelman, D. "Final Version of TOPEX EULERC Subroutine," Fairchild IOC REF: GNC:TOPEX:89-229, 17 October 1989.

## **ACKNOWLEDGEMENTS**

The authors wish to thank the TOPEX/Poseidon Project for the important support we have received enabling us to pursue these advanced T/P nonconservative force models for precision orbit determination. The authors would also like to thank the following individuals for their continued support: S.M. Klosko, R.G. Williamson, D.D. Rowlands, J.J. McCarthy, N.P. Zelensky, and J.L. Wiser.

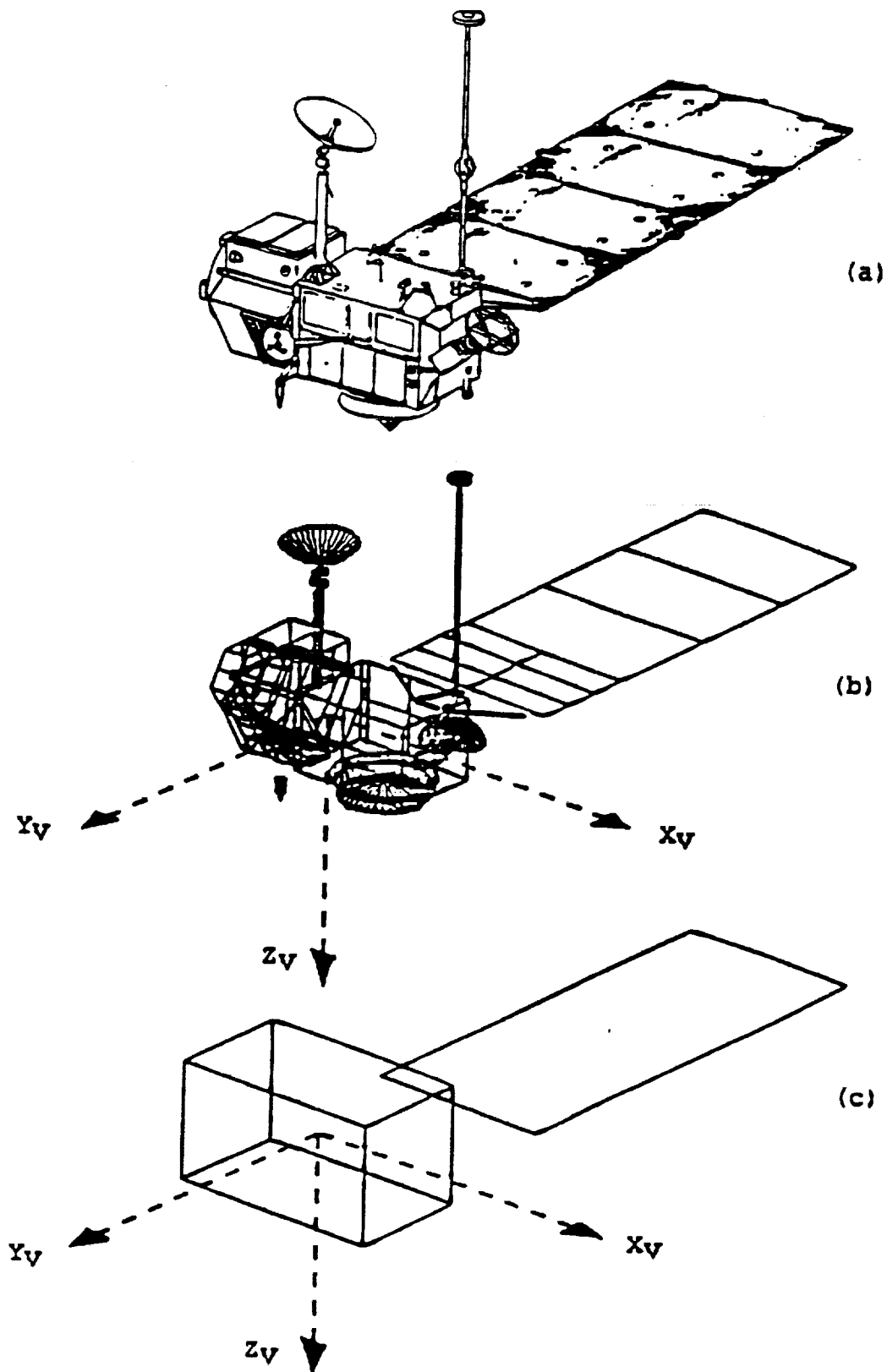


Figure 1. (a) The TOPEX/Poseidon Spacecraft, (b) Micro-Model Approximation, (c) Macro-Model Approximation

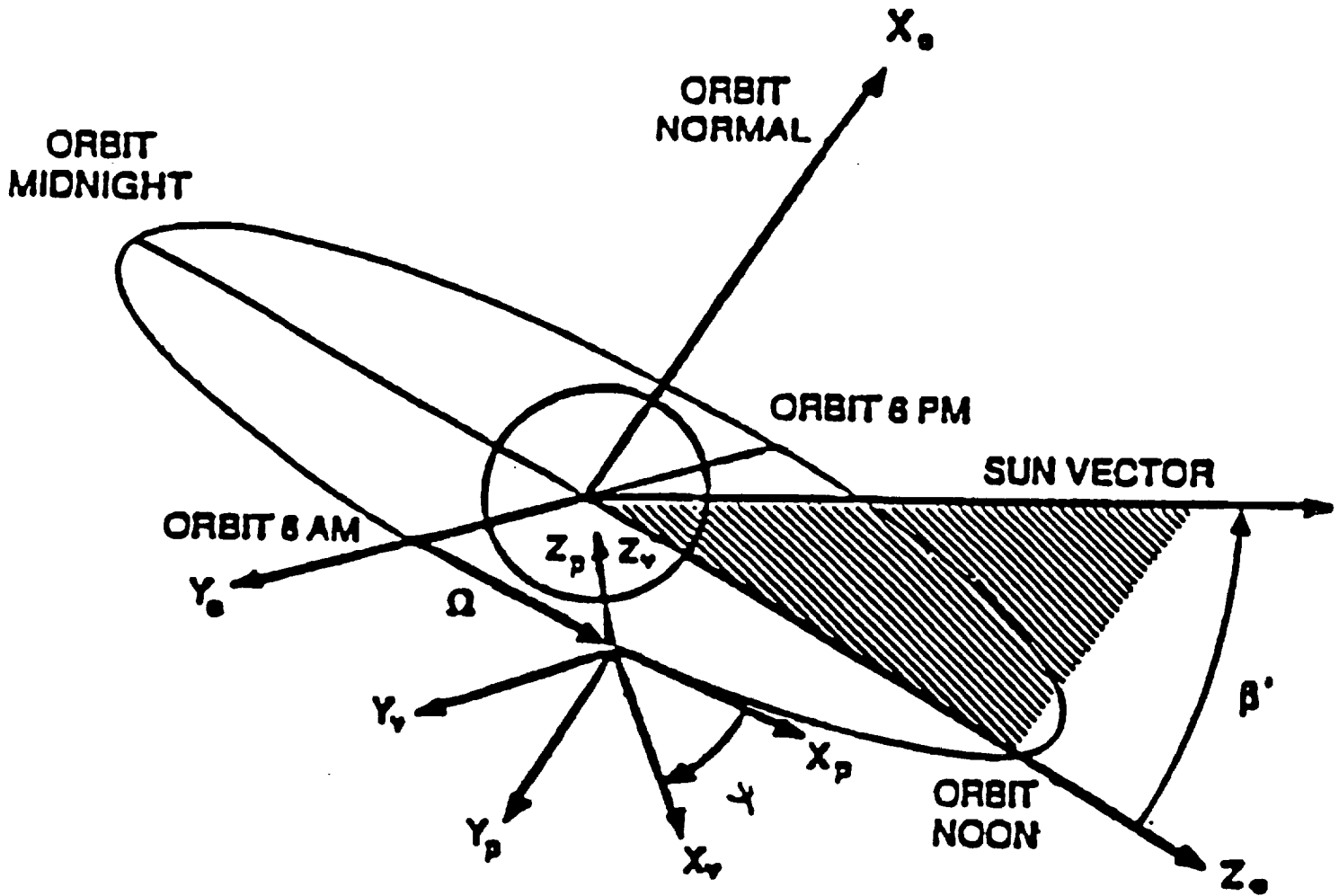


Figure 2. TOPEX/Poseidon Inertial Coordinate System (Perrygo, 1987)

**Table 1. Modelability and Error Analysis Summary**  
(Marshall et al., 1992)

FORCE	RMS of Micro Model Force for B' of 0° to 88° and Orbit Angle of 0° to 360°	RMS of Macro-Micro Model Residuals	RMS Radial 10 Day Orbit Error
Solar Alongtrack	$3.2 \times 10^{-8} \text{ M/S}^2$	$4.3 \times 10^{-9} \text{ M/S}^2$	
Solar Crosstrack	$4.5 \times 10^{-8} \text{ M/S}^2$	$4.3 \times 10^{-9} \text{ M/S}^2$	
Solar Radial	$2.7 \times 10^{-8} \text{ M/S}^2$	$4.9 \times 10^{-9} \text{ M/S}^2$	
Total Radial Orbit Error for 10 Day Arc →			5.1 cm
Albedo Alongtrack	$6.1 \times 10^{-10} \text{ M/S}^2$	$2.3 \times 10^{-10} \text{ M/S}^2$	
Albedo Crosstrack	$8.3 \times 10^{-10} \text{ M/S}^2$	$3.3 \times 10^{-10} \text{ M/S}^2$	
Albedo Radial	$4.6 \times 10^{-9} \text{ M/S}^2$	$2.4 \times 10^{-10} \text{ M/S}^2$	
Total Radial Orbit Error for 10 Day Arc →			2.1 cm
IR Alongtrack	$6.1 \times 10^{-10} \text{ M/S}^2$	$5.4 \times 10^{-10} \text{ M/S}^2$	
IR Crosstrack	$7.4 \times 10^{-10} \text{ M/S}^2$	$5.3 \times 10^{-10} \text{ M/S}^2$	
IR Radial	$5.6 \times 10^{-9} \text{ M/S}^2$	$5.4 \times 10^{-10} \text{ M/S}^2$	
Total Radial Orbit Error for 10 Day Arc →			2.2 cm
Thermal Alongtrack	$2.0 \times 10^{-9} \text{ M/S}^2$	$1.0 \times 10^{-9} \text{ M/S}^2$	
Thermal Crosstrack	$3.6 \times 10^{-9} \text{ M/S}^2$	$5.9 \times 10^{-10} \text{ M/S}^2$	
Thermal Radial	$1.6 \times 10^{-9} \text{ M/S}^2$	$5.5 \times 10^{-10} \text{ M/S}^2$	
Total Radial Orbit Error for 10 Day Arc →			5.2 cm

**Table 2. Baseline Laser Station Configuration and Tracking Schedule**

1) MOBLAS-4	Monument Peak, CA
2) MOBLAS-5	Yarragadee, Australia
3) MOBLAS-7	Greenbelt, MD
4) MOBLAS-8	Quincy, CA
5) TLRs	Cerro Tololo, Chile
6) TLRs	Easter Island, Chile
7) MLRS	Fort Davis, TX
8) HOLLAS	Haleakala, HI
9) MOBLAS-2	Bar Giyyora, Israel
10) SAO-1	Matera, Italy
11) Wettzell	Wettzell, Federal Republic of Germany
12) RGO	Herstmonceux, Great Britain
13) Shanghai	Shanghai, Peoples Republic of China
14) Simosato	Simosato, Japan
15) Orroral	Orroral Valley, Australia

Shift (8 hrs)	DAY										Tracking Obtained
	1	2	3	4	5	6	7	8	9	10	
1st	X	X	X	X	X			X	X	X	40%
2nd			X	X	X	X	X			X	20%

TABLE 3. Orbit Error Due To Radiative Force Model Errors Only (Macro-Micro Model)

Parameterization and Tracking Type	Orbit Error For 10 Day Arc (cm)															
	$\beta' = 0^\circ$ to $29^\circ$				$\beta' = 10^\circ$ to $39^\circ$				$\beta' = 39^\circ$ to $68^\circ$				$\beta' = 67^\circ$ to $88^\circ$			
	RAD	CROSS	ALONG		RAD	CROSS	ALONG		RAD	CROSS	ALONG		RAD	CROSS	ALONG	
Free-Adjust. Parameter Set Nominal Laser Tracking	2.40	0.97	20.03		1.90	1.72	11.70		3.93	6.06	10.08		3.13	2.01	8.04	
Constrained Parameter Set Nominal Laser Tracking	4.27	6.20	21.00		4.52	2.78	16.51		4.39	6.41	22.77		3.22	2.97	11.50	
Constrained Parameter Set Full Laser Tracking	2.51	5.62	15.04		2.80	2.35	13.51		3.64	6.11	11.66		2.99	3.55	7.16	

TABLE 4. Orbit Error Due To Radiative Force Model Errors Only (Macro-Model Clones)

Parameterization, Tracking Type and Error Model	Orbit Error For 10 Day Arc (cm)														
	$\beta' = 0^\circ$ to $29^\circ$				$\beta' = 10^\circ$ to $39^\circ$				$\beta' = 39^\circ$ to $68^\circ$				$\beta' = 67^\circ$ to $88^\circ$		
	RAD	CROSS	ALONG		RAD	CROSS	ALONG		RAD	CROSS	ALONG		RAD	CROSS	ALONG
Free-Adjust. Parameter Set Nominal Laser Tracking. Clone Model 1					0.32	1.47	2.25		0.43	0.58	3.23				
Free-Adjust. Parameter Set Nominal Laser Tracking. Clone Model 2					1.27	3.18	3.88		4.10	2.47	10.52				
Free-Adjust. Parameter Set Nominal Laser Tracking. Clone Model 3					0.59	1.92	3.29		0.37	0.61	3.37				
Constrained Parameter Set Nominal Laser Tracking. Clone Model 1					1.82	1.81	4.48		1.44	1.16	7.99				
Constrained Parameter Set Nominal Laser Tracking. Clone Model 2					2.03	3.75	6.50		3.15	4.83	33.67				
Constrained Parameter Set Nominal Laser Tracking. Clone Model 3					1.18	2.52	4.18		1.10	1.50	6.01				

TABLE 5. Orbit Error Due To Radiative Force (Macro-Micro) and Atmospheric Density (DTM-J71) Model Errors

Parameterization and Tracking Type	Orbit Error For 10 Day Arc (cm)															
	$\beta' = 0^\circ$ to $29^\circ$				$\beta' = 10^\circ$ to $39^\circ$				$\beta' = 39^\circ$ to $68^\circ$				$\beta' = 67^\circ$ to $88^\circ$			
	RAD	CROSS	ALONG		RAD	CROSS	ALONG		RAD	CROSS	ALONG		RAD	CROSS	ALONG	
Reduced Free-Adjust. Parameter Set + $C_p$ /Day. Nominal Laser Tracking.	4.08	13.07	23.90		3.31	11.45	8.91		3.89	7.78	15.98		2.43	1.01	9.53	
Reduced Free-Adjust. Parameter Set + $C_p$ /Day + Once-Per-Rev Along Track General Acceleration. Nominal Laser Tracking.	2.56	4.20	14.53													
Macro-model (no adjust) + $C_p$ /Day + $C_p$ /Arc + Once-Per-Rev Along Track General Acceleration. Nominal Laser Tracking.	1.58	1.34	10.33													
Cannonball + $C_p$ /Day + $C_p$ /Arc + Once-Per-Rev Along Track General Acceleration. Nominal Laser Tracking.	2.05	1.68	6.40													

TABLE 6. Orbit Error Analysis In the Presence of Gravity Error

ERROR MODEL	FORCE MODELING & ADJUSTED PARAMETERS	Orbit Error For 10 Day Arc (cm)			
		$\beta' = 0^\circ$ to $29^\circ$			
		RAD	CROSS	ALONG	DATA FIT
GEMT2-GEMT2C1	Adjusting State Only	23.15	24.36	73.17	
GEMT2-GEMT2C1 + Atmospheric Density Error (DTM-J71) + Radiative Force Error (Macro-Micro)	Macro Model Adjusting State + $C_p$ /Day + Free Adjusting Macro-Model Parameters	13.50	36.26	38.54	25.39
GEMT2-GEMT2C1 + Atmospheric Density Error (DTM-J71) + Radiative Force Error (Macro-Micro)	Cannonball Adjusting State + $C_p$ /Day + $C_r$ /Arc + Once-Per-Rev Along Track General Acceleration	9.71	23.25	70.96	19.56
GEMT2-GEMT2C1 + Atmospheric Density Error (DTM-J71) + Radiative Force Error (Macro-Micro). With data on first day.	Macro Model Adjusting State + $C_p$ /Day + Free Adjusting Macro-Model Parameters	13.34	34.75	36.42	24.77
GEMT2-GEMT2C1 + Atmospheric Density Error (DTM-J71) + Radiative Force Error (Macro-Micro). With data on first day.	Cannonball Adjusting State + $C_p$ /Day + $C_r$ /Arc + Once Per Rev Along Track General Acceleration	9.49	23.45	32.96	19.54
GEMT2-GEMT2C1 + Atmospheric Density Error (DTM-J71) + Radiative Force Error (Macro-Micro). With data on first day.	Macro Model Adjusting State + $C_p$ /Day + Free Adjusting Optimal Set of Macro-Model Parameters	9.20	25.35	32.02	19.42

**TABLE 7. Additional Orbit Error Analysis in the Presence of Gravity Error**

		Orbit Error For 10 Day Arc (cm)		
		$\beta' = 0^\circ$ to $29^\circ$		
ERROR MODEL	FORCE MODELING & ADJUSTED PARAMETERS	RAD	CROSS	ALONG
GEMT2-GEMT2C1 + Atmospheric Density Error (DTM-J71) + Radiative Force Error (Macro-Micro)	Cannonball Adjusting State + $C_p$ /Day	46.20	25.47	171.95
GEMT2-GEMT2C1 + Atmospheric Density Error (DTM-J71) + Radiative Force Error (Macro-Micro)	Macro Model Adjusting State + $C_p$ /Day	343.30	52.92	124.09
GEMT2-GEMT2C1 + Atmospheric Density Error (DTM-J71) + Radiative Force Error (Macro-Micro)	Macro Model Adjusting State + $C_p$ /Day + Constrained Set of Parameters	15.74	32.81	44.34

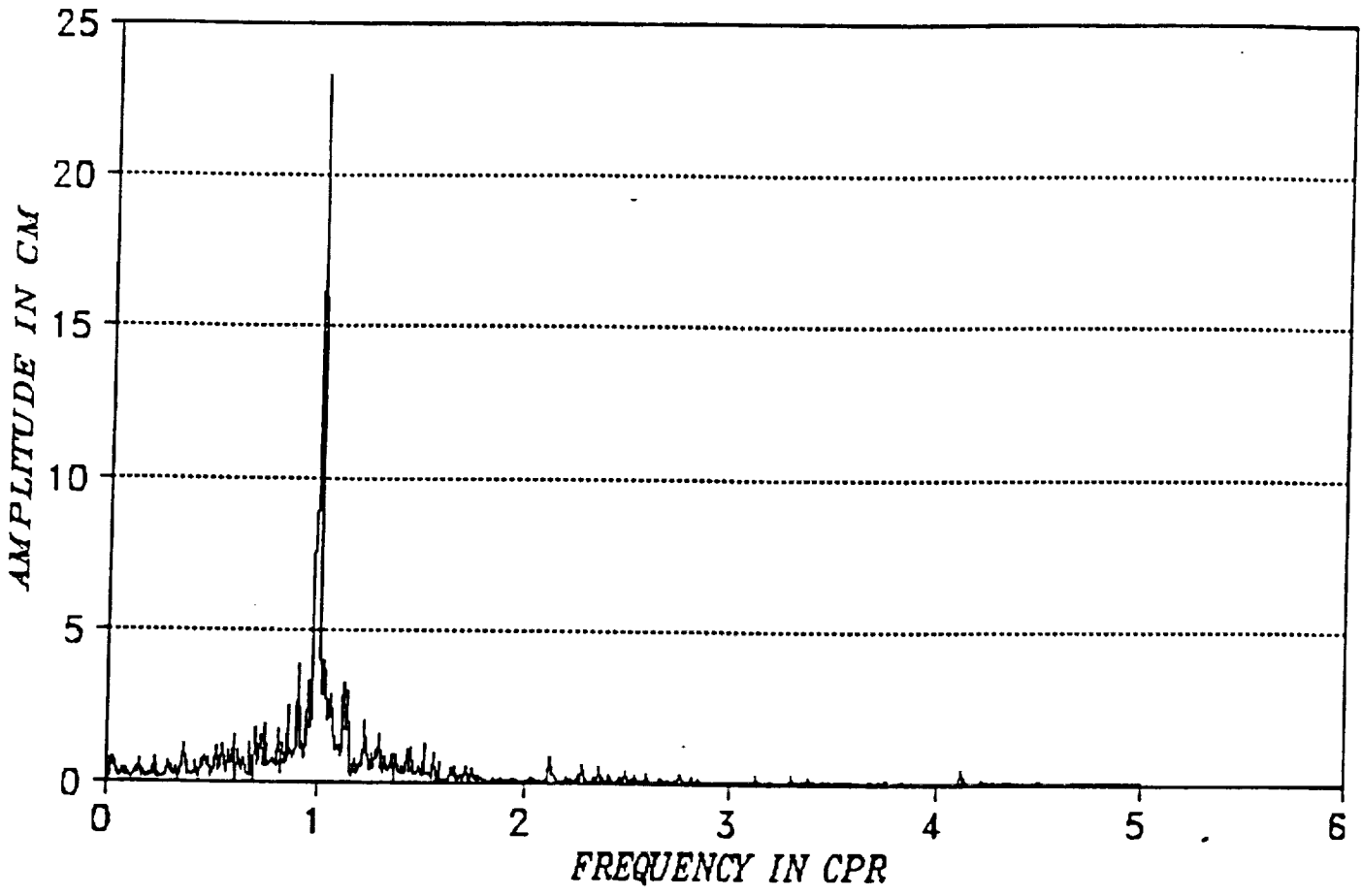


Figure 3. Radial Orbit Error Spectral Characteristics For GEMT2-GEMT2C1 Error

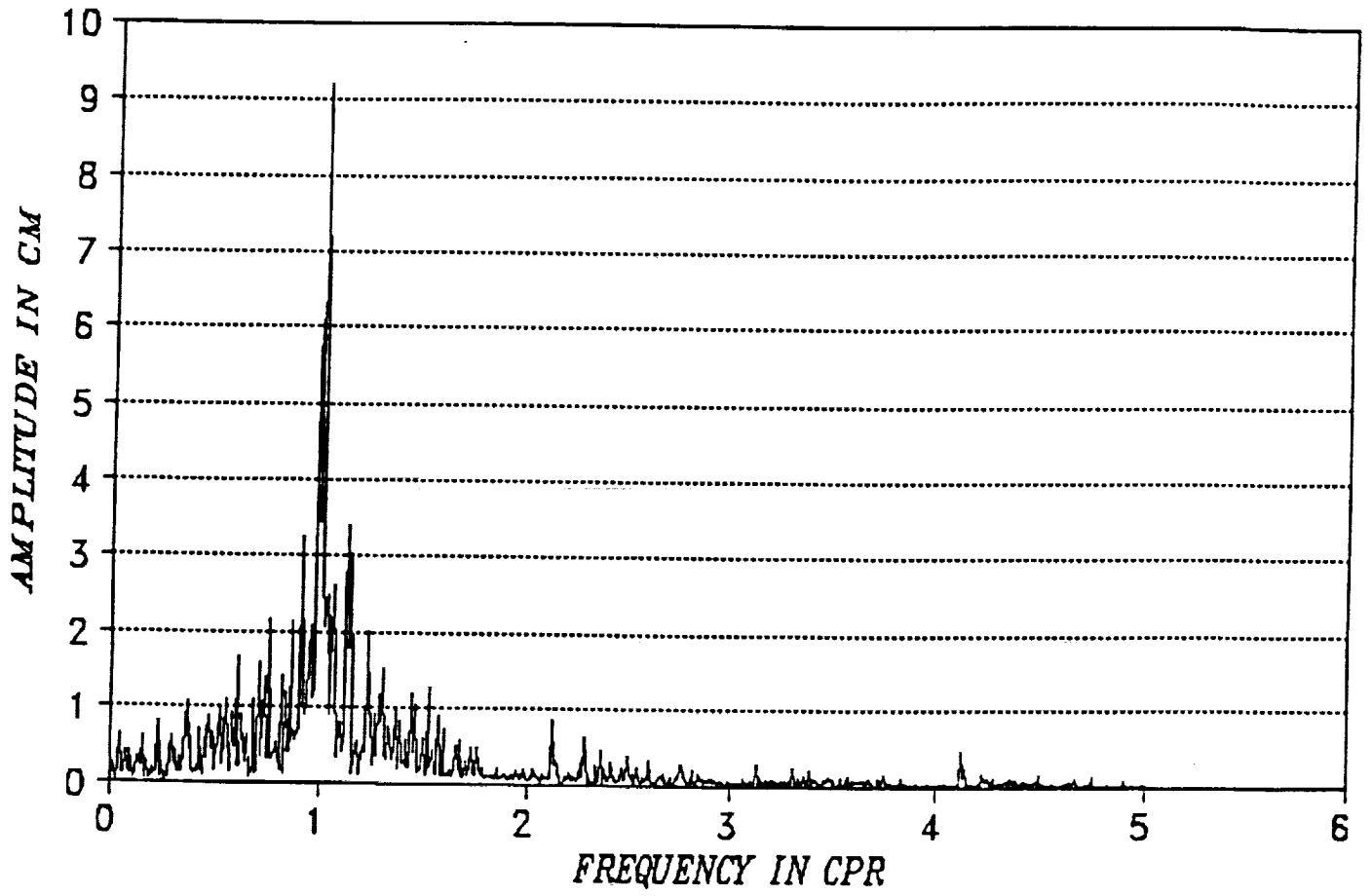


Figure 4. Radial Orbit Error Spectral Characteristics For GEMT2-GEMT2C1 Error + DTM-J71 Error + MACRO-MICRO Radiative Force Error

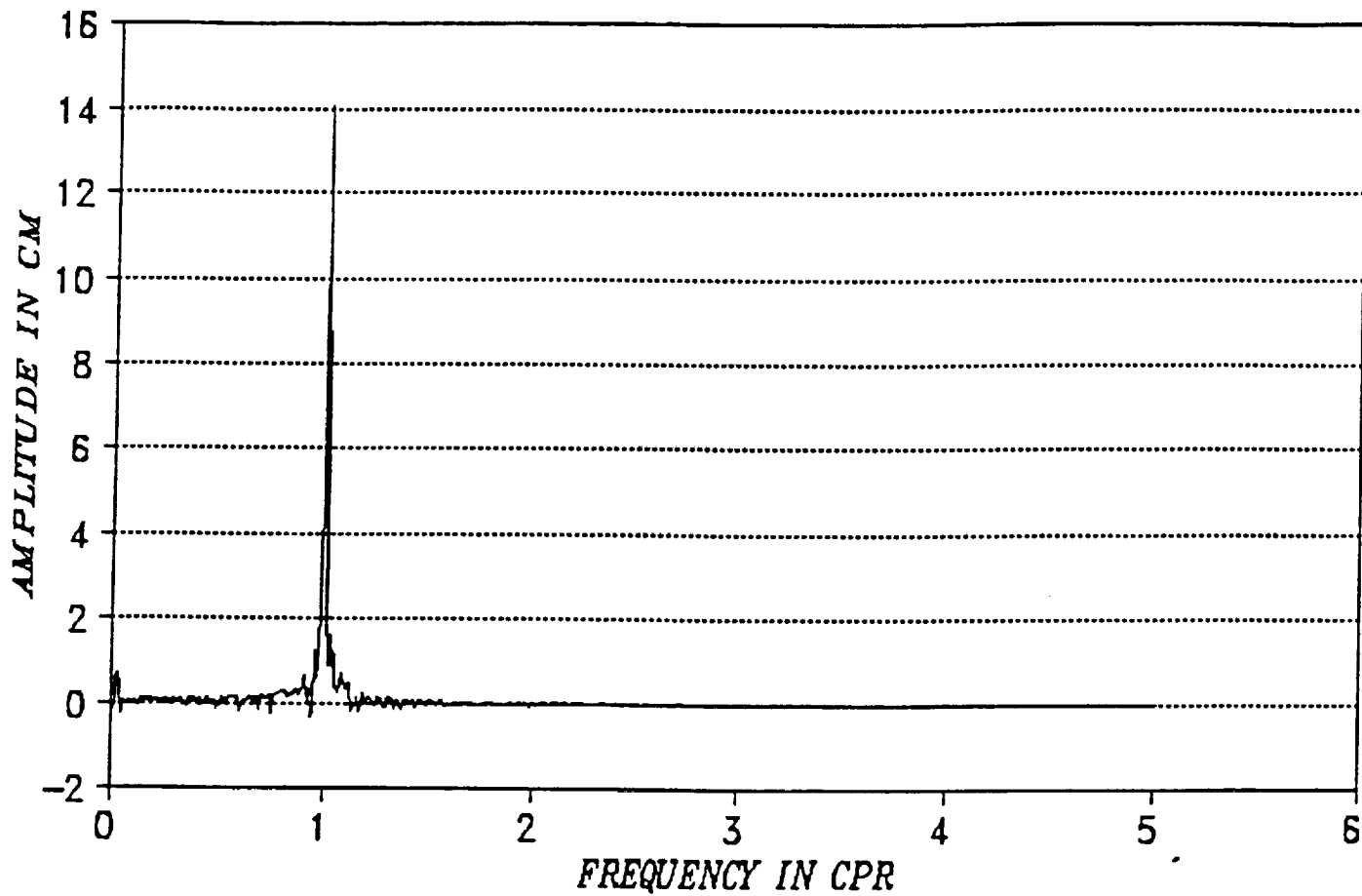


Figure 5. Residuals of Gravity Error Spectrum and Gravity + Drag + MACRO-MICRO Spectrum (Difference Between Figure 4 & Figure 3)

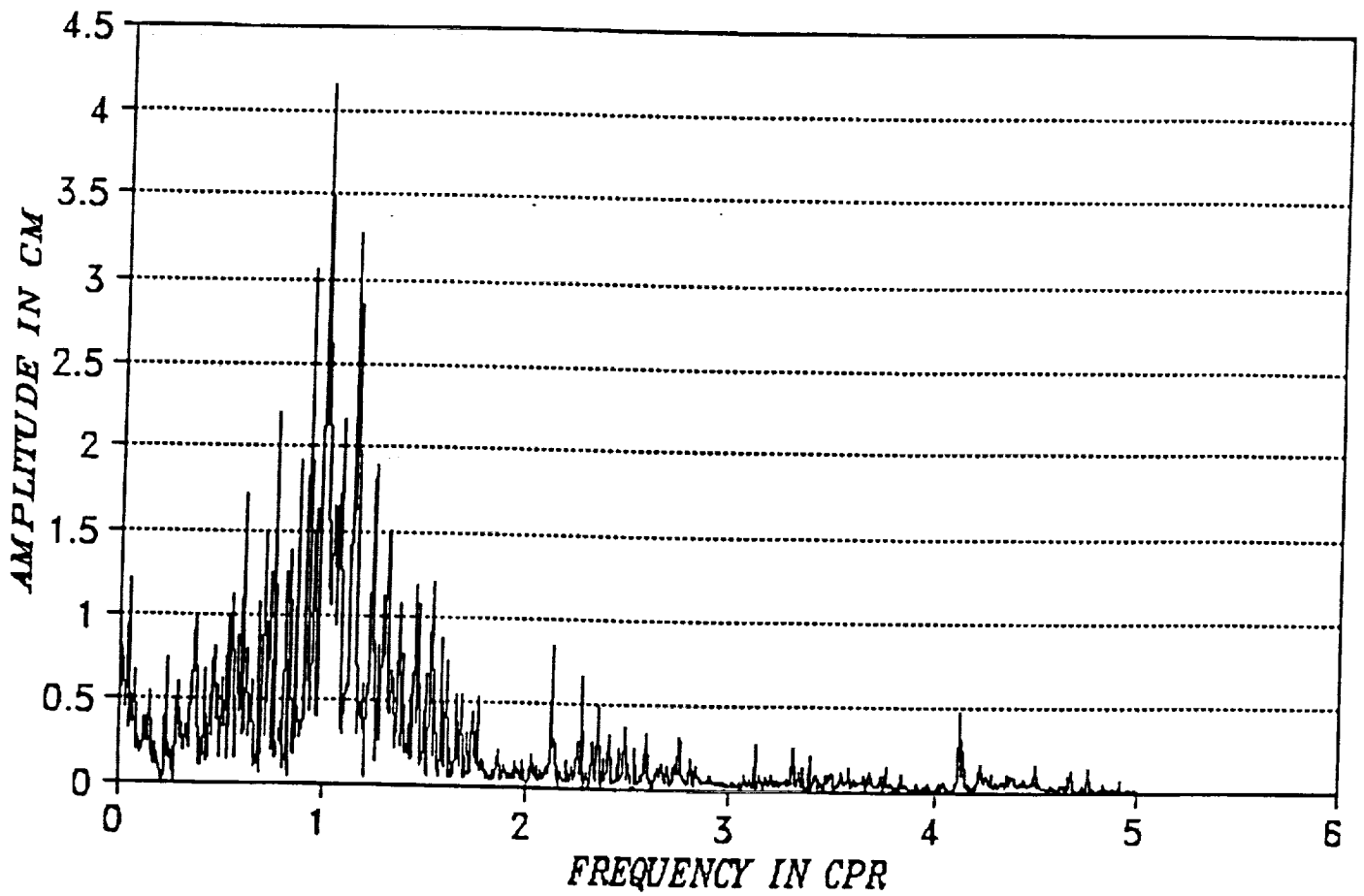


Figure 6. Radial Orbit Error Spectral Characteristics For GEMT2-GEMT2C1 Error + DTM-J71 Error + MICRO-CANNONBALL Radiative Force Error Adjustment of Along Track Once-Per-Rev General Acceleration

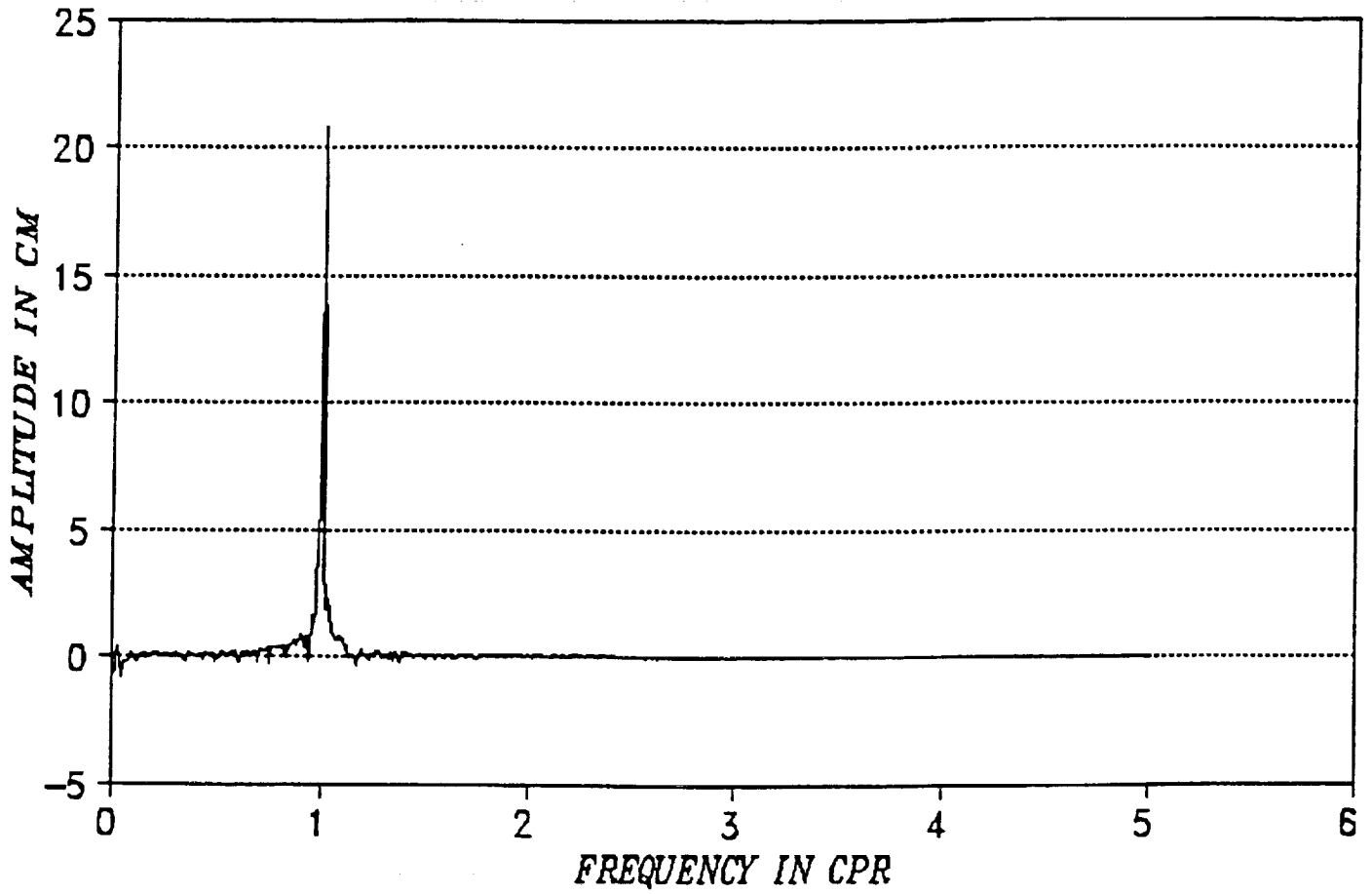


Figure 7. Residuals of Gravity Error Spectrum and Gravity + Drag + MICRO-CANNONBALL With Once-Per-Rev General Acceleration Spectrum (Difference Between Figure 6 & Figure 3)

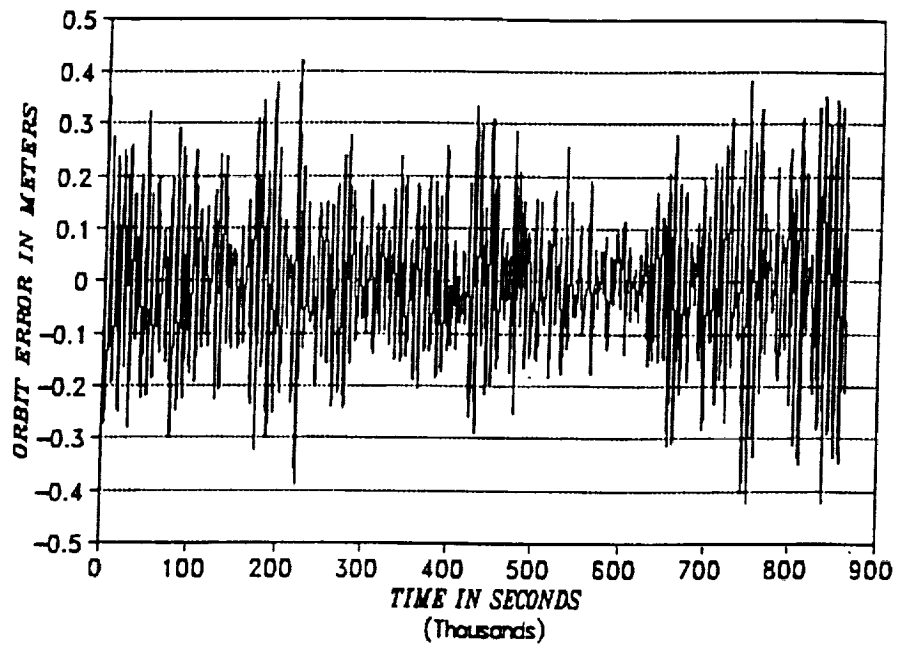


Figure 8. Radial Orbit Error Using Macro-Model Parameterization

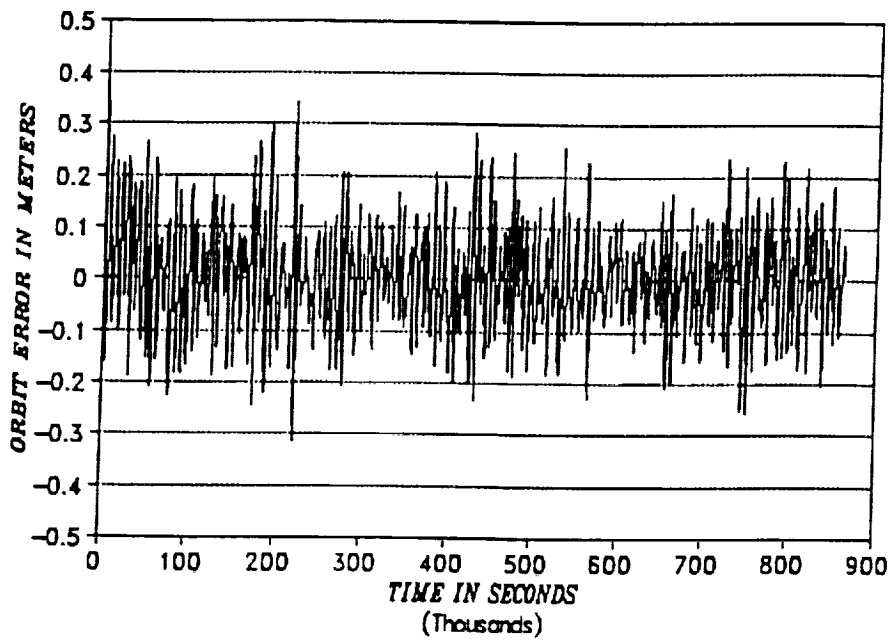


Figure 9. Radial Orbit Error Using Cannonball and Once-Per-Rev Parameterization

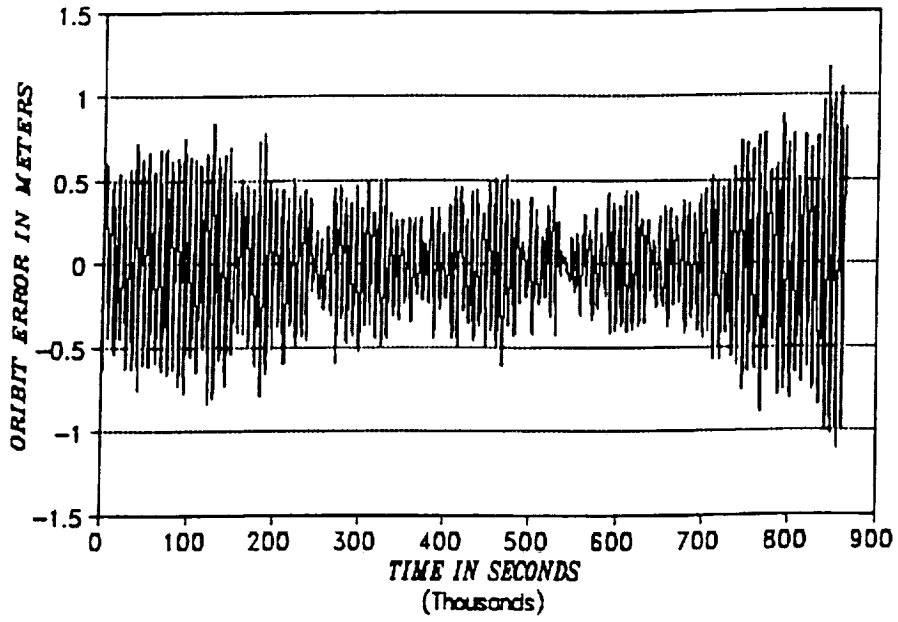


Figure 10. Cross Track Orbit Error Using Macro-Model Parameterization

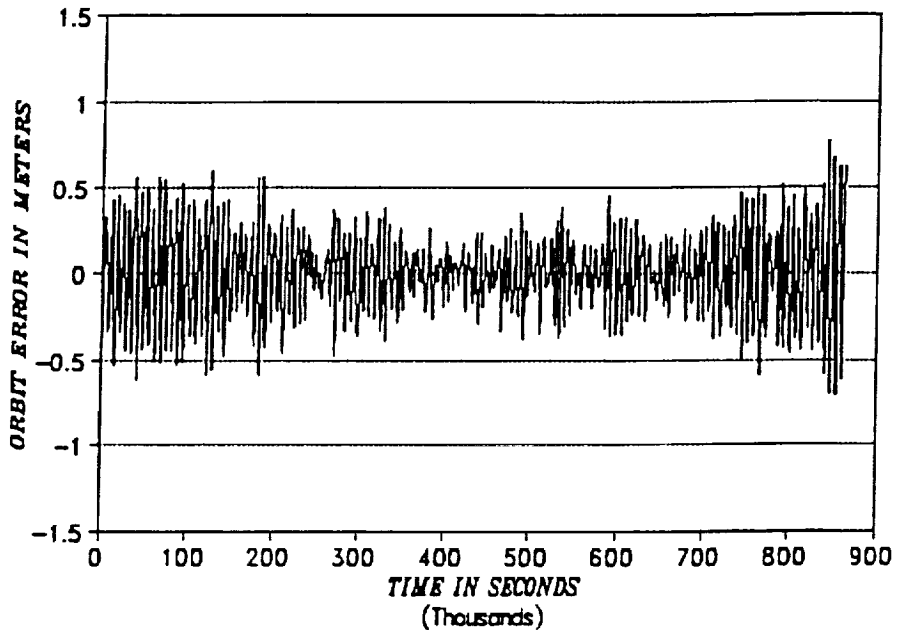


Figure 11. Cross Track Orbit Error Using Cannonball and Once-Per-Rev Parameterization

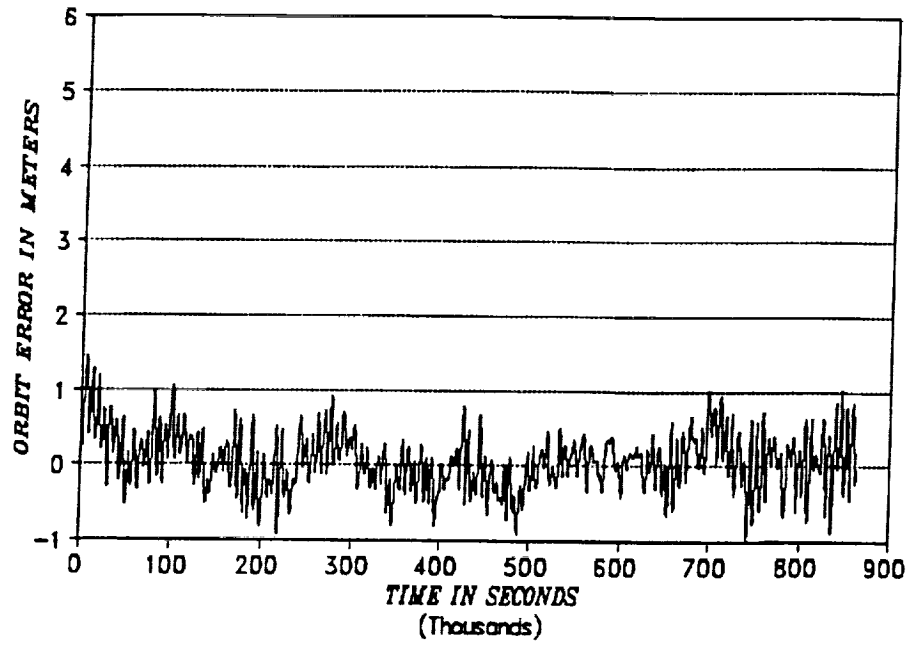


Figure 12. Along Track Orbit Error Using Macro-Model Parameterization

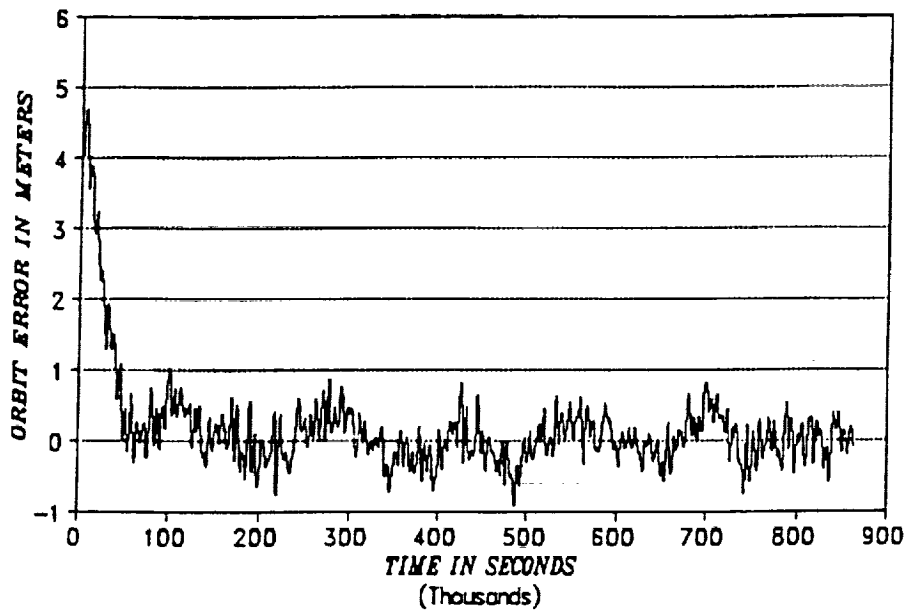


Figure 13. Along Track Orbit Error Using Cannonball and Once-Per-Rev Parameterization

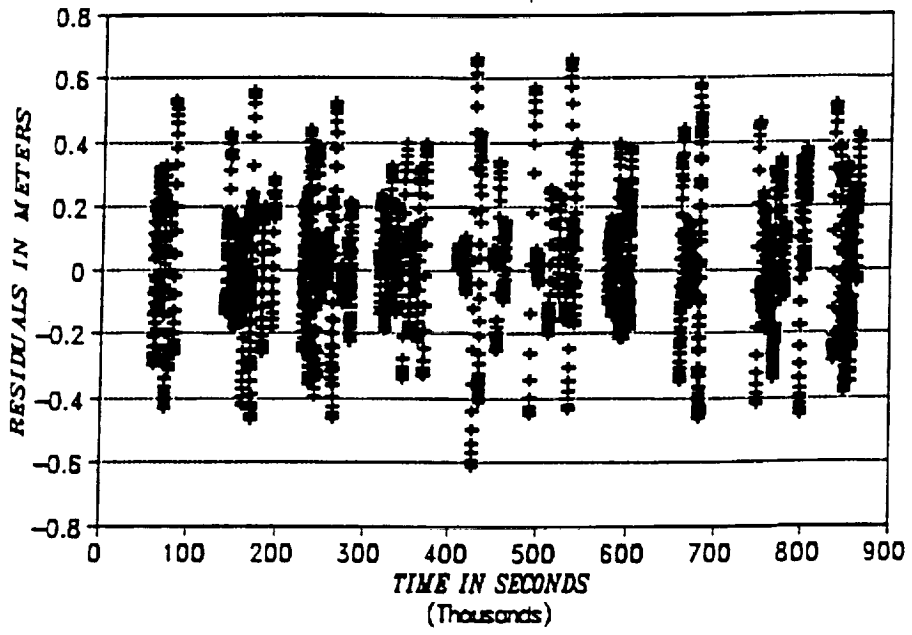


Figure 14. Laser Range Residuals Using Cannonball and Once-Per-Rev Parameterization

## Appendix A. "Box-Wing" Acceleration Equations

### Solar and Earth Radiation

The radiation pressure acting on a flat plate can be computed using the following equation (*Milani et al., 1987*), assuming a Lambertian diffusion,

$$\vec{\Gamma} = -\frac{GA\cos\theta}{Mc} [2(\delta/3 + \rho\cos\theta)\vec{n} + (1-\rho)\vec{s}]$$

where

$\Gamma$	≡	radiation pressure acceleration on the flat plate
$A$	≡	surface area of the flat plate
$\theta$	≡	angle between surface normal and Sun source vectors
$G$	≡	radiation flux from source
$\vec{n}$	≡	surface normal vector
$\vec{s}$	≡	source incidence vector
$\rho$	≡	specular reflectivity (% of total incoming radiation)
$\delta$	≡	diffusive reflectivity (% of total incoming radiation)
$M$	≡	satellite mass
$c$	≡	speed of light

The albedo and infrared accelerations use a similar acceleration equation as the solar radiation. However, the flux magnitude is different. Also, the source vector is the Earth grid spot-to-satellite vector rather than the solar incidence vector. The spot definition and location are defined by *Knocke et al., (1988)*. Note that this model is not self-shadowing. The total albedo/infrared acceleration can be expressed as:

$$\vec{\Gamma} = -\sum_i^N \sum_j^{10} \frac{G_i A_j \cos\theta_j}{Mc} [2(\delta_j/3 + \rho_j \cos\theta_j)\vec{n}_i + (1-\rho_j)\vec{s}_j]$$

where	$i$	≡	plate of interest
	$j$	≡	Earth spot of interest
	$n$	≡	total number of plates

### Spacecraft Radiation

The force exerted on a surface due to thermal emission, assuming a Lambertian diffusion function, can be expressed as:

$$\vec{F} = -\frac{2A\sigma}{3c} \epsilon T^4 \vec{n}$$

where

$\epsilon$	$\equiv$	emissivity
$\sigma$	$\equiv$	Stefan-Boltzmann constant (5.67E-08 W/m <sup>2</sup> /K <sup>4</sup> )
$A$	$\equiv$	surface area
$T$	$\equiv$	temperature (Kelvin)
$c$	$\equiv$	speed of light (m/s)
$n$	$\equiv$	surface normal vector

and while in sunlight

$$T = a + c \cos\left(\frac{\theta}{x}\right) \left[ 1 - \exp\left(-\frac{t_1}{f}\right) \right]$$

and while in shadow as

$$T = a + c \exp\left(-\frac{t_2 + s_2}{d}\right)$$

where

$$s_2 = -d \ln\left(\cos\left(\frac{\theta_{\text{shd}}}{x}\right) \left[ 1 - \exp\left(-\frac{t_1}{f}\right) \right]\right)$$

and

$a$	$\equiv$	cold equilibrium surface temperature
$c$	$\equiv$	delta temp. between cold and hot equilibrium
$d$	$\equiv$	transition time from hot to cold equilibrium temp.
$f$	$\equiv$	transition time from cold to hot equilibrium temp.
$x$	$\equiv$	rotation rate/thermal inertia constant
$t_1$	$\equiv$	time since shadow exit
$t_2$	$\equiv$	time since shadow entry
$s_1$	$\equiv$	shift parameter to ensure continuity
$s_2$	$\equiv$	shift parameter to ensure continuity
$\theta$	$\equiv$	angle between surface normal and solar incidence
$\theta_{\text{shd}}$	$\equiv$	angle between normal and Sun vectors at shadow entry
$\theta_{\text{sun}}$	$\equiv$	angle between normal and Sun vectors at shadow exit

The adjustable parameters are area, emissivity, and all five temperature terms ( $a, c, d, f, x$ ).

# REPORT DOCUMENTATION PAGE

*Form Approved*  
OMB No. 0704-0188

Public reporting burden for this collection of information is estimated to average 1 hour per response, including the time for reviewing instructions, searching existing data sources, gathering and maintaining the data needed, and completing and reviewing the collection of information. Send comments regarding this burden estimate or any other aspect of this collection of information, including suggestions for reducing this burden, to Washington Headquarters Services, Directorate for Information Operations and Reports, 1215 Jefferson Davis Highway, Suite 1204, Arlington, VA 22202-4302, and to the Office of Management and Budget, Paperwork Reduction Project (0704-0188), Washington, DC 20503.

<b>1. AGENCY USE ONLY (Leave blank)</b>	<b>2. REPORT DATE</b> November 1992	<b>3. REPORT TYPE AND DATES COVERED</b> Technical Memorandum
<b>4. TITLE AND SUBTITLE</b>  Nonconservative Force Model Parameter Estimation Strategy for TOPEX/Poseidon Precision Orbit Determination		<b>5. FUNDING NUMBERS</b>  926
<b>6. AUTHOR(S)</b>  S. B. Luthcke and J. A. Marshall		<b>8. PERFORMING ORGANIZATION REPORT NUMBER</b>  93B00013
<b>7. PERFORMING ORGANIZATION NAME(S) AND ADDRESS(ES)</b>  Laboratory for Terrestrial Physics Goddard Space Flight Center Greenbelt, Maryland 20771		<b>10. SPONSORING/MONITORING AGENCY REPORT NUMBER</b>  TM-104575
<b>9. SPONSORING/MONITORING AGENCY NAME(S) AND ADDRESS(ES)</b>  National Aeronautics and Space Administration Washington, D.C. 20546-0001		<b>11. SUPPLEMENTARY NOTES</b>  S.B. Luthcke: Hughes STX Corporation, Lanham, Maryland. J.A. Marshall: NASA-GSFC, Greenbelt, Maryland.
<b>12a. DISTRIBUTION/AVAILABILITY STATEMENT</b>  Unclassified - Unlimited Subject Category 14		<b>12b. DISTRIBUTION CODE</b>
<b>13. ABSTRACT (Maximum 200 words)</b>  The TOPEX/Poseidon spacecraft was launched on August 10, 1992 to study the Earth's oceans. To achieve maximum benefit from the altimetric data it is to collect, mission requirements dictate that TOPEX/Poseidon's orbit must be computed at an unprecedented level of accuracy. To reach our prelaunch radial orbit accuracy goals, the mismodeling of the radiative nonconservative forces of solar radiation, Earth albedo and infrared re-radiation, and spacecraft thermal imbalances cannot produce in combination more than a 6-cm rms error over a 10-day period. Similarly, the 10-day drag modeling error cannot exceed 3-cm rms. In order to satisfy these requirements, a "box-wing" representation of the satellite has been developed in which the satellite is modelled as the combination of flat plates arranged in the shape of a box and a connected solar array. The radiative/thermal nonconservative forces acting on each of the eight surfaces are computed independently, yielding vector accelerations which are summed to compute the total aggregate effect on the satellite center-of-mass. Select parameters associated with the flat plates are adjusted to obtain a better representation of the satellite acceleration history. This study analyzes the estimation of these parameters from simulated TOPEX/Poseidon laser data in the presence of both nonconservative and gravity model errors. A "best choice" of estimated parameters is derived and the ability to meet mission requirements with the "box-wing" model is evaluated.		
<b>14. SUBJECT TERMS</b>  Orbit Calculation, Geodesy, TOPEX/Poseidon, Solar Radiation, Earth Albedo, Spacecraft Thermal Properties, Nonconservative Forces, Finite Element Analysis, Modeling		<b>15. NUMBER OF PAGES</b>  42
<b>17. SECURITY CLASSIFICATION OF REPORT</b>  Unclassified		<b>16. PRICE CODE</b>
<b>18. SECURITY CLASSIFICATION OF THIS PAGE</b>  Unclassified	<b>19. SECURITY CLASSIFICATION OF ABSTRACT</b>  Unclassified	<b>20. LIMITATION OF ABSTRACT</b>  Unlimited